Nanoscale

PAPER

View Article Online
View Journal | View Issue

Cite this: *Nanoscale*, 2016, **8**, 10659

Helical graphene oxide fibers as a stretchable sensor and an electrocapillary sucker†

Chunfei Hua,[a] Yuanyuan Shang,*[a] Xiying Li,[b] Xiaoyang Hu,[c] Ying Wang,[a] Xinchang Wang,[a] Yingjiu Zhang,[a] Xinjian Li,[a] Huiling Duan[b] and Anyuan Cao*[d]

Received 13th March 2016,
Accepted 20th April 2016

DOI: 10.1039/c6nr02111e

www.rsc.org/nanoscale

Fibers made from carbon nanotubes or graphene are strong and conductive; encoding helical structures into these fibers may render useful properties such as high stretchability. Here, we directly spin freestanding graphene oxide (GO) films into helical fibers consisting of uniformly arranged loops with tunable diameters, under controlled environmental humidity. Reduced GO fibers with a helical shape are stretched elastically with a reversible electrical resistance change for many strain cycles. Stretchable temperature sensors built on helical fibers work at large strains (up to 50%) and high temperature (up to 300 °C), with a reliable deformation-independent response. The GO fibers also contain through-channels inside with suitable pore size, which can take up an aqueous electrolyte quickly under a low bias, resulting in a fiber-shaped, on–off switchable electrocapillary sucker. Our multifunctional helical and hollow GO fibers have potential applications in stretchable fiber-shaped sensors, actuators and nano-fluid systems.

Introduction

Macroscopic, continuous fibers made from carbon nanotubes (CNTs) or graphene have shown a wide range of applications in electronics, sensors, actuators, energy and environmental areas.[1–13] Graphene-based fibers represented an emerging research field and were fabricated from exfoliated graphene oxide (GO) sheets by methods such as wet-spinning a liquid-crystalline dispersion,[14–18] hydrothermal cross-linking,[19,20] and dry-film scrolling.[21] Nanomaterials including CNTs and Ag nanowires were introduced into the GO solution to spin reinforced fibers with improved mechanical and electrical properties.[22–25] There were many efforts in tailoring the fiber structure, for example, by freeze-drying wet-state GO fibers which produced internally oriented pores,[26] and by coaxial two-capillary wet-spinning which resulted in hollow tubes that may find use in micropumps and catalysis.[27] However, current wet-spun GO fibers usually adopted a straight shape with limited stretchability. Hence, recently reported stretchable conductive wires or strain sensors were mainly based on buckled GO fibers or dip-coated GO sheets adhered on elastomer substrates, rather than using freestanding fibers.[25,28,29] Encoding helical structures into the originally straight GO fibers, as already done in CNT yarns,[30–32] would be a desired way to overcome the challenge and facilitate the design and construction of high performance stretchable and wearable electronics.

Wet-spinning techniques generally produced straight rather than helical-shaped fibers, since it would be difficult to apply torsional force on the extruded GO solution and dried GO fibers tend to break upon large-degree twisting. Previously, we directly fabricated helical CNT yarns consisting of uniform micro-loops by spinning a piece of the as-grown single-walled nanotube spiderweb.[30] Recently, a dry-film scrolling method was adopted to spin GO fibers which could be self-coiled over a finite length.[21] However, only a small number of helical loops could be embedded in the straight portion, making it difficult to explore relevant properties and applications.

Previously, only straight GO yarns have been synthesized and their applications as stretchable nano-textiles are rather limited. Here, we report self-coiled (*versus* straight) GO fibers with uniform microstructure and tunable diameter, enabling novel applications such as fiber-shaped stretchable sensors and water suckers. We successfully encode uniformly arranged GO loops along the entire length of the fiber by a humidity-assisted freestanding strip-scrolling process, whereas the conventional dry film scrolling method only produces a small number of helical loops along the straight fiber. The resulting helical GO fibers were elastic within moderate tensile strains, with a reversible electrical resistance change during cyclic stretching. We thus constructed a stretchable temperature

[a]*School of Physical Engineering, Zhengzhou University, Zhengzhou, Henan 450052, China. E-mail: yuanyuanshang@zzu.edu.cn*
[b]*Department of Mechanics and Engineering Science, College of Engineering Peking University, Beijing 100871, P. R. China*
[c]*College of Science, Henan Institute of Engineering, Zhengzhou, Henan 451191, China*
[d]*Department of Materials Science and Engineering, College of Engineering, Peking University, Beijing 100871, P. R. China. E-mail: anyuan@pku.edu.cn*
†Electronic supplementary information (ESI) available. See DOI: 10.1039/c6nr02111e

sensor working at a wide strain and temperature range and producing a stable response that was independent of the fiber deformation. Compared with over-twisted CNT helical yarns, the GO fibers made by scrolling flat strips have a unique through-channel structure internally, thus we also built an electrocapillary sucker to take in an aqueous electrolyte under low voltage in an on–off controllable manner. The related mechanism for electrocapillary suction was analyzed.

Results and discussion

The fabrication process of helical and chemically reduced GO (rGO) fibers involved the following steps (as illustrated in Fig. 1a, see the Experimental section for details). First, a *ca.* 2 wt% aqueous GO solution (sheet sizes of 150–200 μm, ESI, Fig. S1†) was delivered onto a polytetrafluoroethylene plate, spread by using a cylindrical rod, dried and then lifted off as a freestanding film (area of 450 cm^2) (Fig. 1b). The thickness of the wet GO coating was defined by the raised adhesive tapes (0.1–0.2 mm) at the two ends of the rod, and after complete drying it decreased to an appropriate range (1 to 2 μm) for easy lift off. A roller blade was used to cut the dry film into narrow strips with smooth edges, while the strip width (1 to 10 mm) would determine the diameter of the as-spun fibers. A smooth edge was important since macroscopic defects or fluctuation of the strip width would cause undesired fracture during subsequent spinning. Both the large-area film and cut strips

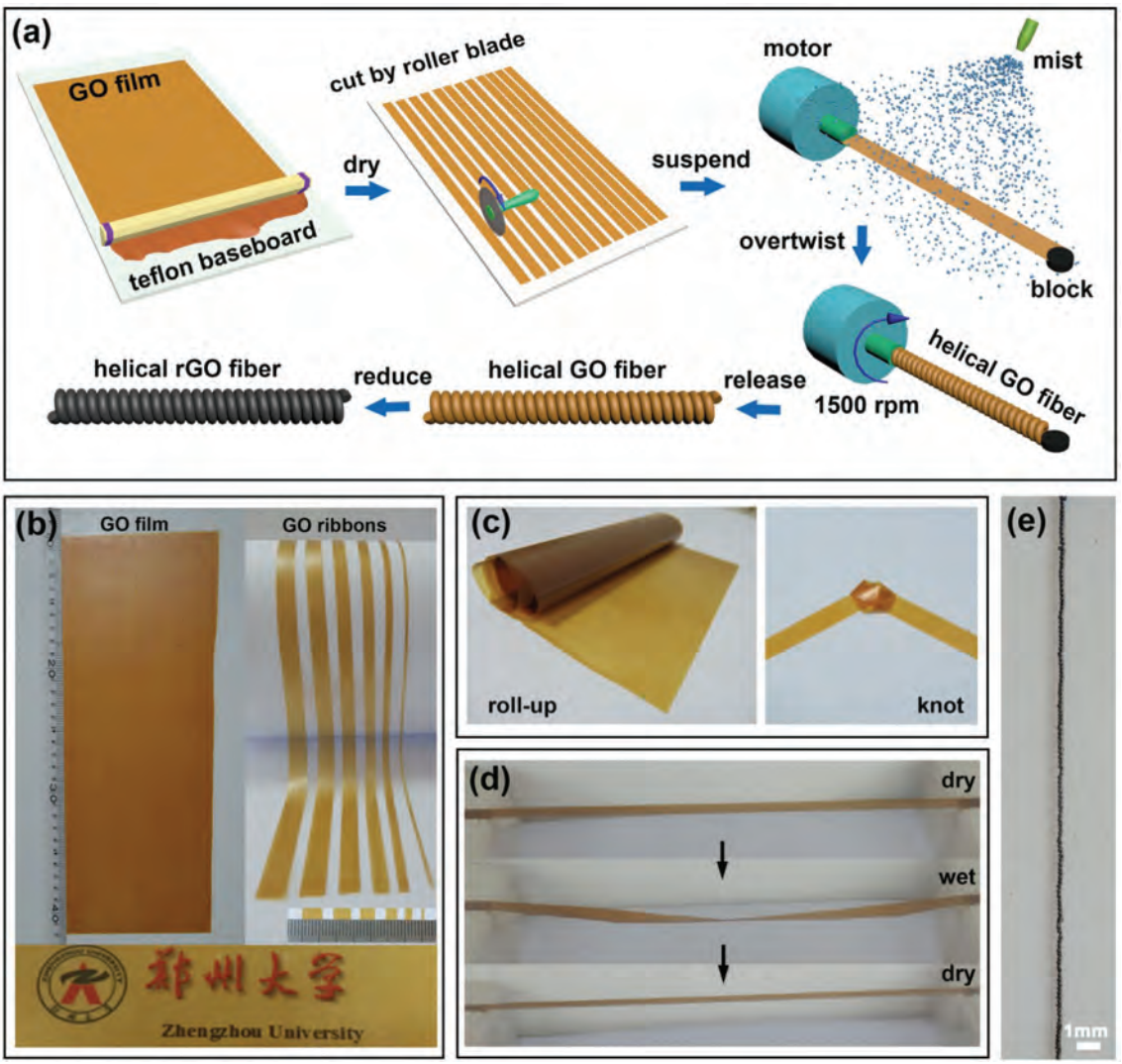

Fig. 1 Fabrication of helical GO and rGO fibers. (a) Illustration of the process involving: (1) spreading a GO solution over a Teflon plate and drying into a solid film, (2) cutting the film into strips with different widths by using a roller blade, (3) applying humidity by mist spraying, (4) spinning the suspended strip into a helical fiber, and (5) converted into rGO fibers by chemical reduction. (b) Photos of a 450 mm^2 dried GO film and cut strips with widths of 1 to 6 mm, and a transparent film placed on the logo of Zhengzhou University. (c) A rolled-up GO film and a strip made into simple knots. (d) A suspended GO strip which became sagged and slightly curled after applying a humidity of 80%, and straightened again in the dry state. (e) Photo of a 24 mm long freestanding helical rGO fiber.

showed certain flexibility, and could be rolled up or made into simple knots (Fig. 1c).

Those GO strips were suspended and twisted by using an electrical motor, similar as the dry-film scrolling process reported earlier.[21,30] However, the processability of GO strips was relatively poor compared with more flexible single-walled nanotube yarns. Here, we found that a suitable environmental humidity and relatively fast spinning (~1500 revolutions per minute) were critical factors for successful over-twisting and formation of helical structures over a long fiber length; the strips tended to break during the process under less or little humidity. We applied a desired humidity (80%–90%) around the GO strip by mist spraying for a while (30 s), and then carried out the fast spinning process immediately. At this humidity, the initially straightened GO strip became sagged and slightly curled, a favorable condition to avoid premature breaking during subsequent twisting (Fig. 1d). The sagged strip was straightened again when it was dried completely, indicating that the humidity-induced shape change in the GO strips was a reversible process. Water adsorption by the hydrophilic GO strips was the main reason for the observed volume expansion and self-curling. Here, a controlled humidity introduced by mist spraying is the key factor for obtaining uniformly coiled GO fibers along the entire length without early breaking, whereas the previous dry film scrolling method usually produces only a short coiled segment in the fiber.[21] Previously, we obtained helical CNT yarns by over-twisting a piece of nanotube spiderweb.[30] Likewise, here the GO strip was converted to a helical fiber through continued over-twisting, and generally we obtained 3–5 cm long freestanding fibers in which tiny helical structures could be distinguished by the naked eye (Fig. 1e).

After HI treatment, the fiber color changed from brown (for GO fibers) to black (rGO), and the resulting rGO fibers showed an electrical conductivity of ~50 S cm^{-1} which could be further improved by doping or thermal annealing. Raman and X-ray diffraction characterization on the GO and rGO films (before spinning) revealed a certain increase of the 2D band after HI reduction and a corresponding decrease of the inter-sheet distance from 8.26 Å (2θ = 10.7°) down to 3.65 Å (2θ = 24.4°), indicating the removal of functional groups and closer stacking of GO sheets (Fig. S2†). We also fabricated helical rGO fibers with different lateral sizes (loop diameters) ranging from 150 to 500 μm, as characterized by scanning electron microscopy (SEM) images (Fig. 2a). Along each fiber, the helical loops had similar sizes indicating a rather uniform microstructure, while small gaps were present between adjacent loops, and the loops were slightly tilted (with an angle of ~60°) along the fiber axis. Statistical measurement on 30 helical fibers revealed a linear relationship between the straight fiber diameter (d) and loop diameter (D, which is larger than d due to the helical path) as $D \approx 1.46d$ (Fig. S3†).

The surface topography of helical GO and rGO fibers was characterized by high-magnification SEM images. Fig. 2b shows a 13.5 mm long GO fiber containing 70 loops through the length (~5 loops per mm), in which d = 137 μm and D = 250 μm. On the loop surface, many wrinkles along the twisting direction were observed, which represent a typical morphology of GO films/coatings dried from a suspension. After chemical reduction, the rGO fibers show similar morphology and maintain the initial helical structure (Fig. 2c). There seemed to be traces of inward collapsing on the loop surface (some local regions appear to be flattened), indicating closer packing of rGO sheets due to a decrease of the inter-sheet distance during reduction. Both the GO and rGO fibers possessed a continuous and smooth surface (skin), a distinct morphology created by the dry-film scrolling.

Mechanical and electromechanical tests on these helical-shaped GO and rGO fibers revealed some distinct properties. As seen from the uniaxial tensile stress–strain (σ–ε) curves, the GO fibers generally reached strains of ε = 20% to 30% before fracture (Fig. 3a). Larger fracture strains (ε = 40% to 50%) were observed in the rGO fibers, but accompanied by reduced modulus (Fig. S4a†), and their ultimate strengths were generally very low (<10 MPa) due to the following reasons. First, the dry-film scrolling method produced GO fibers with large diameters (100–500 μm) with hollow cavities, thus weaker than wet-spun thinner yet very dense fibers. Second, the stress concentration was more severe in over-twisted helical structures compared with straight fibers. We observed that the helical loops were stretched and separated from each other during continuous elongation. It was the loop separation that produced and accommodated such significant deformation, and a helical rGO fiber could be stretched to large tensile strains (ε = 60%) without breaking (Fig. 3b). A flat cross-section was revealed after tension fracture, indicating a brittle failure following loop separation (Fig. S4b†). In comparison, previously reported dry-scrolling GO fibers with straight shape and thinner diameters (d < 200 μm) also showed brittle fracture, whereas those with bigger diameters (d > 340 μm) exhibited a different mechanism, characterized by progressive helical crack propagation from the fiber surface to the core, resulting in a cone-shaped fracture surface (after reduction, the fracture strains reduced significantly).[21] In addition, the helical shape resulted in structure elasticity and the fibers could be repeatedly stretched like a spring within moderate strain. Static uniaxial tension tests on GO and chemically reduced rGO fibers at different strains (ε = 10% and 20%) revealed considerable hysteresis between loading and unloading curves during initial cycles, and the rGO fiber produced a residual strain of ~7% at the second cycle (Fig. 3c and d). So why do the helical rGO fibers typically have lower modulus and are more flexible than GO fibers? The modulus (or spring constant) of the helical fibers is enabled by the ease of loop separation, which is different from the behavior of the other straight GO and rGO fibers (modulus determined by the interaction between GO sheets). Since the loop morphology remains similar in GO and rGO fibers under SEM, we propose that the reduction process (immersing in HI acid at 90 °C for 12 hours) may release some torsional stress in the twisted loops induced during fabrication, thus the loops can be separated more easily (leading to lower modulus and larger strain).

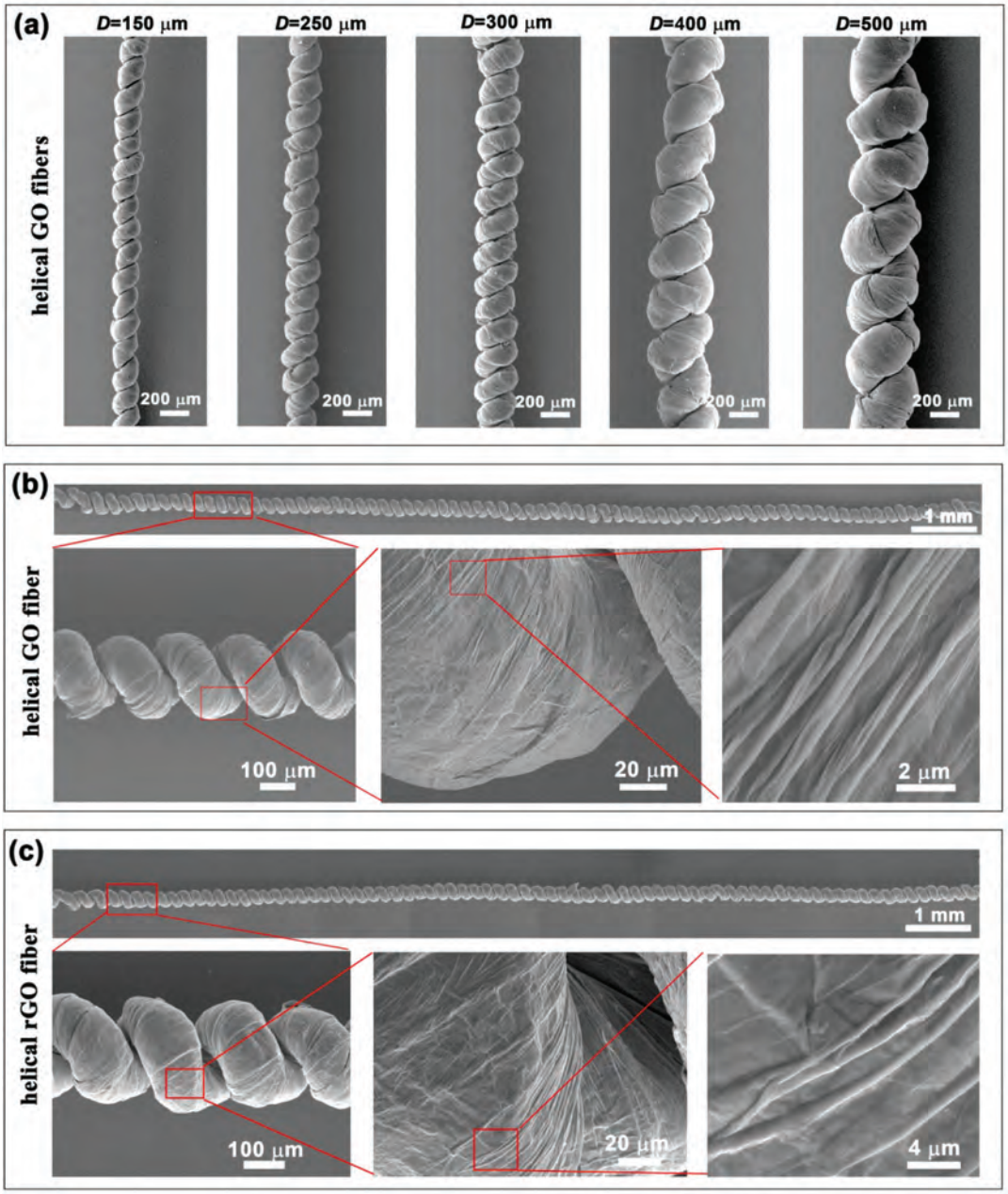

Fig. 2 Structural characterization of helical GO and rGO fibers. (a) SEM images of helical GO fibers with uniform loops and different diameters (from 150 to 500 μm). There is no intentional control on the left-handed or right-handed chirality during spinning; all the samples were spun in the same rotation direction. (b) SEM image of a 13.5 mm long GO fiber, and high-magnification images showing wrinkled surface morphology. (c) SEM images of the same fiber in (b) after chemical reduction.

This is also proved by the fact that we could feel that the fibers became soft after chemical reduction.

Since the helical rGO fibers were conductive and also elastic within moderate strains, we performed electromechanical tests by simultaneously recording the two-probe electrical resistance during cyclic stretching. The fiber resistance (over a gauge length of 1 cm) decreased from initially 287.5 Ω to 279.6 Ω at a tensile strain of ε = 20%, and then increased to ~294 Ω after complete unloading (Fig. 3e). Since the fibers were made by scrolling a piece of dry GO film, empty space existed between the curved film exhibiting a porous cross-section morphology.[21] When the fiber was stretched and loops separated, the lateral shrinking caused by Poisson's ratio would reduce such space and enhance the contact between curved film portions. This in turn decreased fiber resistance upon stretching. Such a resistance change was repeated for 1000 cycles, with periodic oscillation between the maximum value at ε = 0 (~294 Ω) and the minimum value at ε = 20% (~277 Ω) (Fig. 3f). Since the loop separation was mainly responsible for the deformation, the induced resistance change (about 5%) was

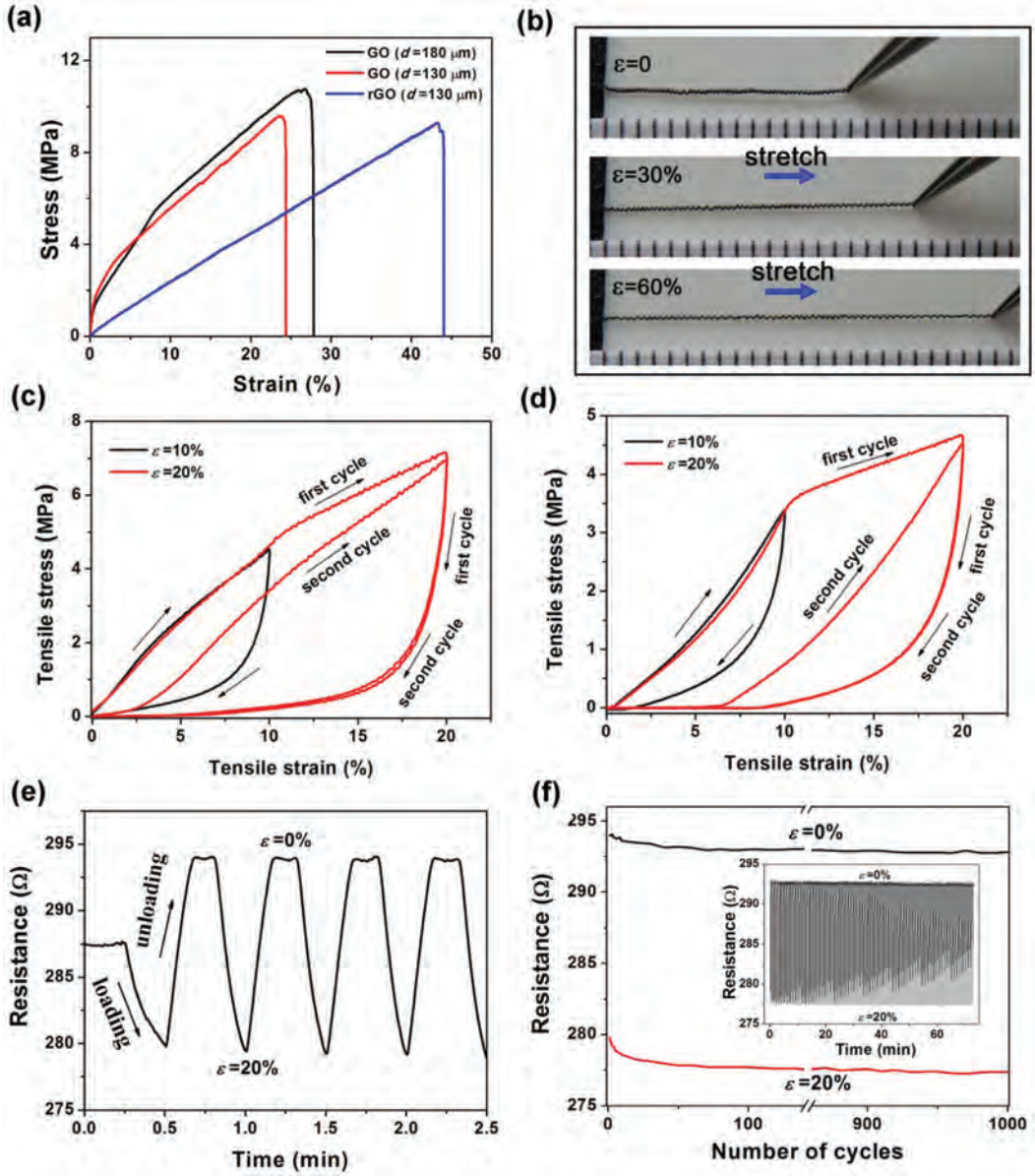

Fig. 3 Mechanical and electrical properties of helical rGO fibers. (a) Tensile stress–strain curves for two GO fibers and a rGO fiber with different diameters. (b) Photos of a helical rGO fiber stretched by using a tweezer to strains of 30% and 60%, respectively. (c) Static cyclic tensile stress–strain curves of a GO fiber stretched to maximum strains of 10% to 20% (two cycles), respectively. (d) Static cyclic tensile stress–strain curves of a chemically reduced rGO fiber. (e) Electrical resistance recorded over 5 cycles during repeated stretching between ε = 0 and 20%. (f) Oscillation of the fiber resistance at two strain limits (ε = 0% and 20%) over 1000 cycles showing reversible resistance change during repeated stretching.

relatively small, but could be highly reversible over many cycles. This property is promising in developing stress or strain sensors, as well as stretchable devices.

Prompted by the above results, we configured a helical rGO fiber-based temperature sensor which could work at either relaxed or stretched states. It relied on a single rGO fiber placed on a hot plate (as the heat source) with electrical wiring at two ends to monitor the resistance change during the heating or cooling process (Fig. 4a). When the entire fiber (a length of 1.5 cm) was heated uniformly, the relative change of resistance ($\Delta R/R_0$, where R_0 is original resistance at room temperature, T = 30 °C) was recorded *in situ*. In a relaxed form, the fiber showed a stable resistance of 193 Ω at 30 °C, which was decreased to 188 Ω upon heating to 100 °C, corresponding to a $\Delta R/R_0$ of −2.6% (Fig. 4b). The value of $\Delta R/R_0$ increased to −5.4% and −10.4% for ultimate heating temperatures of 200 and 300 °C, respectively. The negative proportional R–T relationship indicated a semiconductor behavior dominated by carrier hopping among the stacked rGO sheets, as also observed in graphene fibers by other groups.[33,34] After that, we stretched the helical rGO fiber to a large strain (ε = 50%), and observed similar sensing behavior during heating to different

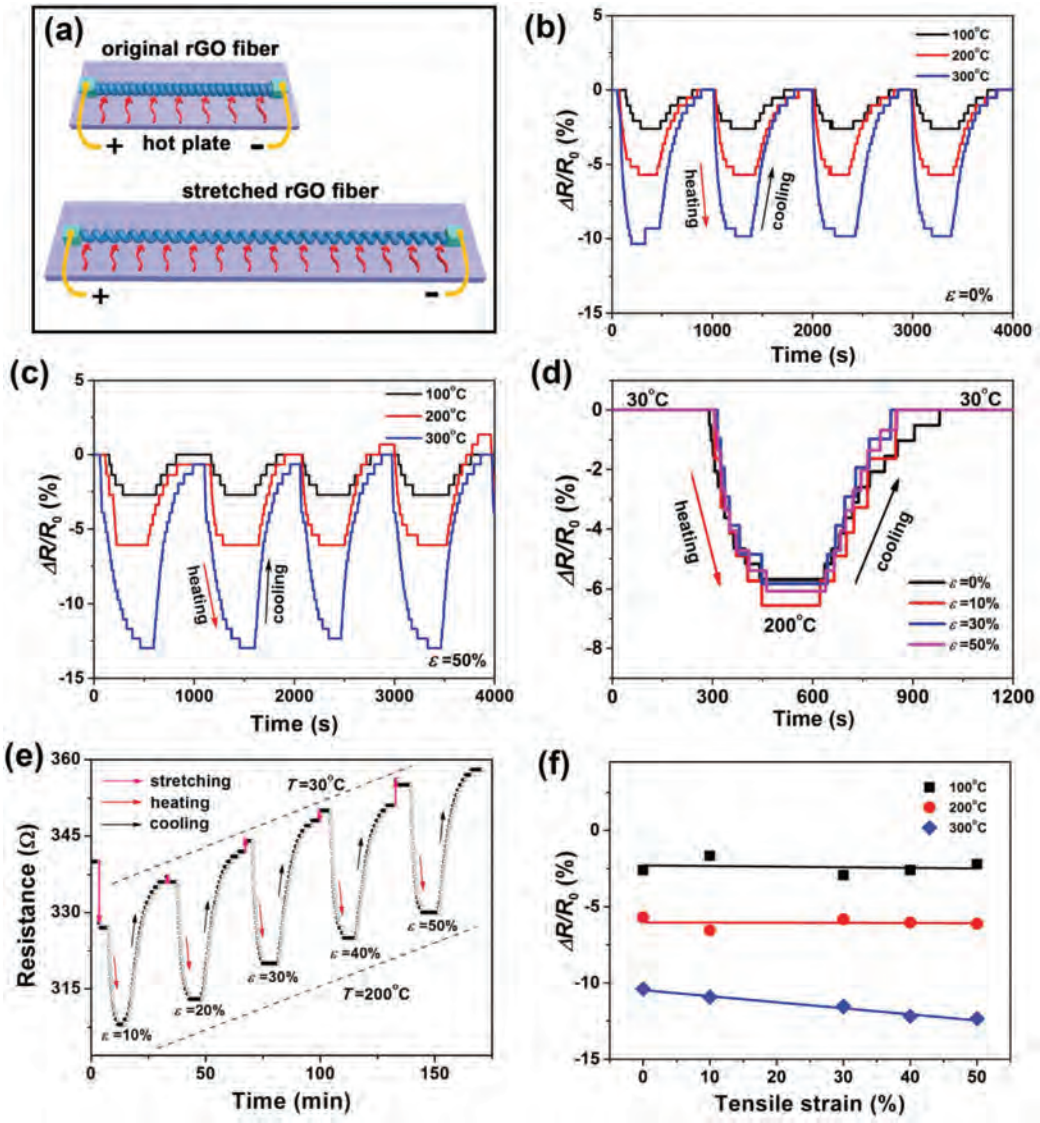

Fig. 4 Helical rGO fibers as temperature sensors. (a) Illustration of the sensor configuration in which a (stretched) fiber was placed on a hot plate. (b) Relative resistance change in an un-stretched fiber during heating and cooling cycles from room temperature to 100, 200 and 300 °C, respectively. (c) Relative resistance change in a pre-stretched fiber (to ε = 50%) during heating and cooling cycles. (d) Relative resistance change in a helical fiber stretched to different strains (ε = 0, 10%, 30%, 50%, respectively) during one heating/cooling cycle (between 30 and 200 °C). (e) Recorded resistance during heating and cooling a helical fiber (between 30 and 200 °C) for 5 cycles (the fiber was stretched to a specific strain at each cycle). (f) Calculated resistance change in the same fiber stretched to strains of ε = 0–50% and heated to temperatures of 100, 200 and 300 °C, respectively.

target temperatures (100, 200, 300 °C), with reproducible resistance change during heating and cooling cycles (Fig. 4c). We also compared the response of this rGO sensor by stretching the fiber to different strains from ε = 0 to 50%; the evolution of $\Delta R/R_0$ was independent of specific strains within the tested range (Fig. 4d).

To further confirm the strain-independent sensing behavior, we carried out a dynamic testing protocol by stretching a fiber sensor to a different strain each time and applying a heating/cooling cycle (between room temperature and 200 °C) at that particular strain (Fig. 4e). For example, a rGO fiber was first stretched to ε = 10% (R decreased from ~340 to 327 Ω), then heated to 200 °C (R further dropped to 308 Ω) and cooled to room temperature (R increased to nearly initial value). In the second cycle, the fiber was stretched to ε = 20% and subjected to the same heating/cooling process. The process was repeated until the fiber reached a large strain (ε = 50%). One could see that the resistance change was quite reproducible, yielding nearly constant $\Delta R/R_0$ values at different strains in response to environmental temperature up to 100 and 200 °C, respectively (Fig. 4f). For even higher temperature (300 °C), the absolute value of $\Delta R/R_0$ showed a gradual increase (from −10.4% to −12.4%) for larger deformation (from ε = 0 to 50%). The above results indicate that our helical rGO fibers work as

stretchable temperature sensors with a stable response under different deformation conditions.

When the dry GO film was scrolled into a fiber, empty space was contained within the fiber and formed through-fiber channels, as indicated by the unique cross-sectional morphology.[21] Based on this through-channel structure, we constructed a fiber-shaped graphene sucker which could take in water from one (bottom) end to the other end, controlled by an applied electrical potential (illustrated in Fig. 5a, see the Experimental section for details). Electrocapillary imbibition in nanoporous Au and CNT sponges was reported by our team and collaborators,[35,36] but it remained unclear whether such a graphene fiber could perform the same function. We cut rGO fibers into 2–3 cm long segments to expose their internal channels, and dipped the open end into the aqueous electrolyte. At this stage, water cannot enter the fiber channel naturally. As the applied potential increased above the threshold voltage (about −0.8 V), the electrolyte started to be sucked in as evident from the linear increase of the sample mass (an electrolyte-infiltrated fiber is much heavier than an empty fiber) (Fig. 5b). This phenomenon was similar to electrocapillary imbibition by CNT sponges, although here the rGO fibers yielded slightly higher threshold voltage. Continuing the imbibition process (at −1.2 V) resulted in a monotonic increase of fiber mass and gradual saturation after several minutes (200 to 400 s) (Fig. 5c). Upon saturation, the mass change (relative to the initial fiber mass) reached about 600–700%, indicating that a rGO fiber had taken in more than 6 times of its own

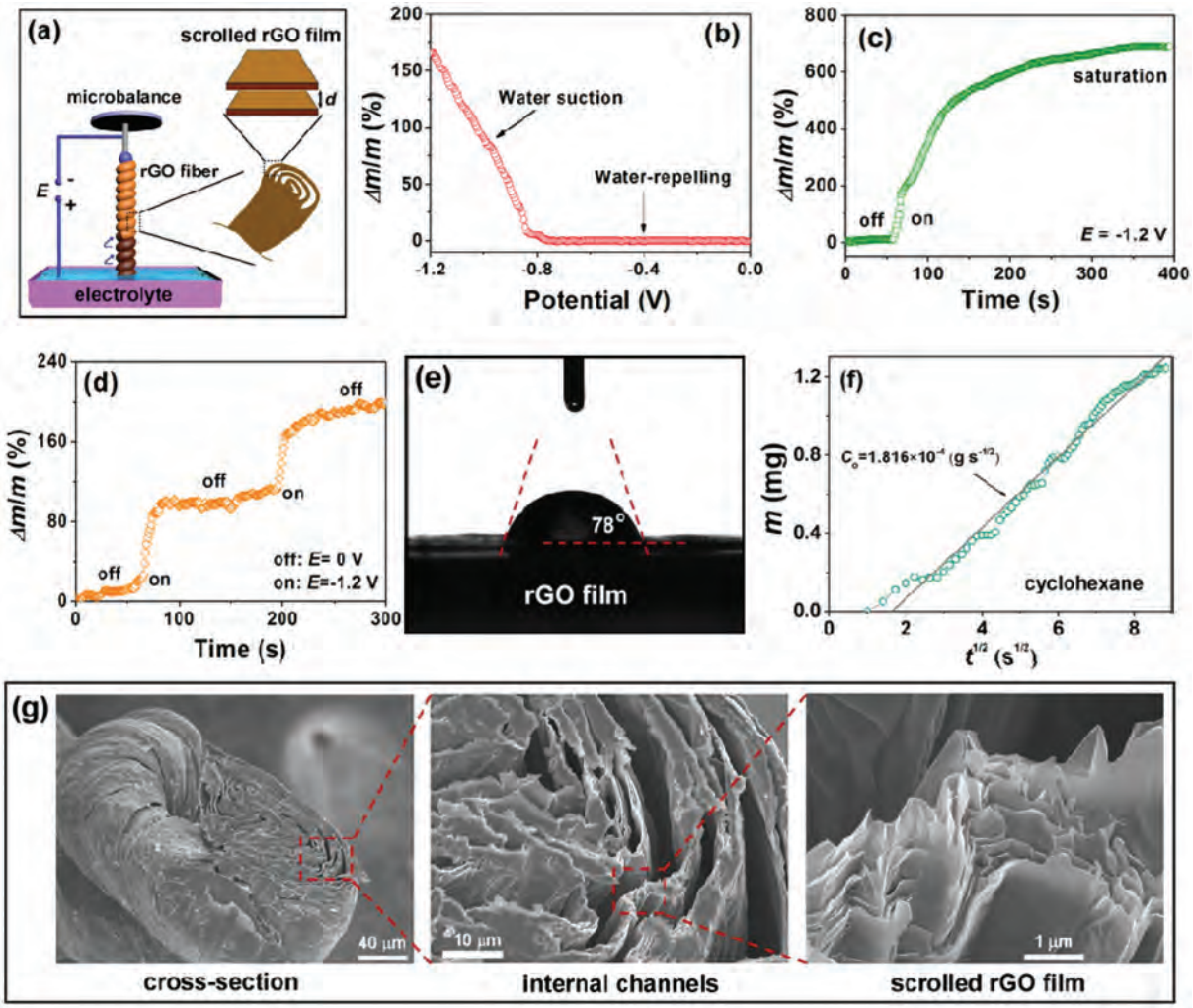

Fig. 5 Electrocapillary suction by helical rGO fibers. (a) Illustration of the setup in which an rGO fiber was suspended under a microbalance and the fiber end was in contact with the electrolyte (1 M KOH). A bias E was applied on the Cu wire connecting the rGO fiber. Inset shows the internal through-channel structure made from the scrolled film, with a distance "d" between scrolled film portions. (b) Recorded fiber relative mass change ($\Delta m/m$) when sweeping the potential from 0 to −1.2 V (5 mV s^{-1}), revealing a threshold voltage of about −0.8 V in order to initiate electrolyte suction. (c) Continued electrocapillary suction process under −1.2 V until saturation. (d) On–off switching of electrolyte suction by applying two potentials (E = 0 and −1.2 V) alternatively during the process. (e) Contact angle (78°) of a water droplet on a planar rGO film. (f) Mass change *versus* time (square rooted) recorded during spontaneous oil imbibition. (g) SEM images of a cut helical fiber cross-section showing parallel internal channels created between the scrolled rGO film.

weight of water. The imbibed water should go through the inner channels as the outer surface was not wet (tested by filter paper) after the imbibition process.

Furthermore, the electrolyte imbibition in our rGO fibers could be switched "on" and "off" by the applied bias. During the process, the relative mass change increased rapidly under a potential of $E = -1.2$ V (corresponding to the "on" state in which water was flowing into the fiber continuously), which was immediately shut off by removing the voltage (Fig. 5d). During the "off" state, the mass change was negligible, indicating that the electrolyte front within the fiber channels had stopped moving upward. The on/off states were repeated by alternating two different potentials ($E = 0$ or -1.2 V) periodically. In this regard, the rGO fibers containing nanoscale inner pipes acted as a fast and efficient (large capacity) electrocapillary sucker, and water suction could be turned on and off controllably. The -1.2 V is a suitable voltage for KOH electrolyte, without producing hydrolysis or degrading the material properties, as demonstrated in carbon nanotube sponges.[36] If there are functional groups generated under high voltage, then the entire graphene fiber should possess those groups thus the surface wetting properties would change correspondingly. But here the mass increase is very large and water suction could be turned off and on controllably, thus removing the influence of functional groups.

In order to estimate the effective channel size (d, empty space formed due to the dry film twisting) within an rGO fiber, we carried out spontaneous oil (cyclohexane) imbibition in the same fiber and plotted the mass change (m) *versus* the square root of time (t) (Fig. 5f). Based on the model of planar Poiseuille flow, the electrocapillary imbibition through the space between two plates can be described by the kinetic formula:[37]

$$h = \frac{m}{\phi\rho A} = \sqrt{\frac{\gamma\cos\theta d}{3\eta}}t, \text{ therefore, } m = \phi\rho A\sqrt{\frac{\gamma\cos\theta d}{3\eta}}t = C\sqrt{t} \quad (1)$$

where h is the height of the rising electrolyte (or oil) front, ρ is the density (1.05 g cm^{-3} for the aqueous electrolyte, and 0.78 g cm^{-3} for oil), A is the cross-sectional area of the fiber (0.2 mm^2 given a fiber diameter of 0.5 mm), γ is the surface tension of water or oil, θ is the contact angle between water (or oil) and the rGO surface, d is the through-channel size or spacing among the twisted rGO film (illustrated in Fig. 5a), η is the viscosity (1.05 mPa s for the aqueous electrolyte, 0.99 mPa s for oil) and ϕ is the porosity. Thus, the proportionality, C in eqn (1), is dependent on the fiber cross-sectional area and physical properties of the imbibed liquid. Fitting the m–t (square rooted) curve yielded a slope of C. For spontaneous oil imbibition, the oil–rGO contact angle could be treated as $\theta = 0$. Therefore, from the oil imbibition data (Fig. 5f, $C \approx 1.8 \times 10^{-4}$ (g s$^{1/2}$)) and eqn (1), we obtained an effective channel size on the order of $d \approx 100$ nm. SEM characterization on the cross-section of a cut rGO fiber revealed internal cavities (gaps) between the scrolled rGO film formed during the spinning process; these are parallel through-channels extending along the entire fiber length (Fig. 5g). Significant over-twisting was applied onto the helical fibers during fabrication, which was critical for obtaining tightly arranged film scrolls and narrow channels in-between for efficient electrocapillary imbibition.

Based on the water imbibition result shown in Fig. 5c (which was then converted to m–$t^{1/2}$ plot), and by taking a channel size of 100 nm, we calculated a water–rGO contact angle of $\theta \approx 46°$ for the imbibed water within the fiber during the "on" state. This value was smaller than the macroscopically measured contact angle (77°–78°) by placing a water droplet on rGO films (before scrolling) (Fig. 5e). The reduction of contact angle indicated enhanced affinity between water and rGO as a bias was applied, which was favorable for water suction. Although electrocapillary imbibition in nano-porous gold and carbon nanotube sponges has been studied,[35,36] here we use a flexible graphene fiber rather than bulk porous materials. Furthermore, their porous structures are different. The nano-porous gold was formed by electrochemical corrosion of the Ag–Au alloy with a bicontinuous structure, and the nanotube sponges contain interconnected pores among a three-dimensional nanotube network. In comparison, our thin rGO fibers possess a unique through-channel structure inside (formed during film scrolling) which facilitates fast and controllable electrolyte suction and transport along the fiber. These graphene-based fiber-shaped water pumps or valves might be integrated into wearable textiles and micro/nano fluid systems for a variety of applications.

Conclusions

In summary, we fabricate helical GO and rGO fibers by spinning thin graphene oxide films under controlled humidity. These fibers contain uniform loops and high stretchability. Based on their helical shape and through-channel structure, a deformation-independent temperature sensor and an electrocapillary sucker have been demonstrated. Fabrication of helical GO/rGO fibers with much larger lengths might also be realized in the traditional wet-spinning process by extruding flat GO ribbons continuously,[38] and simultaneously applying twists. In the future, other materials such as CNTs might be introduced into the GO film to improve the processability and make hybrid helical fibers with tailored electrical and mechanical properties. Also, other materials such as nanoparticles or polymers that are more sensitive to a temperature change might be introduced into the rGO fibers to enhance the sensor response (resistance change). The internal through-channel structure, including the channel shape and size, also could be engineered for exploring electrocapillary applications.

Experimental section

Synthesis of GO sheets

Graphene oxide was prepared from expanded graphite by a modified method based on Hummers' method, with improved

efficiency of the oxidation process, easy temperature control and without generating toxic gas.[39] In the first step, expanded graphite (5 g) and $KMnO_4$ (25 g) were slowly added into a mixture of 360 mL of H_2SO_4 and 40 mL of H_3PO_4 placed in an ice bath. After mechanical stirring for 2 hours, the suspension was placed in a 40 °C water bath and continually stirred for another 5 hours. Then, the dark brown mud mixture was cooled to room temperature and dispersed in 600 mL deionized water in an ice bath. After that, 50 mL 30% H_2O_2 was added into the mixture and allowed to stand for one night for sufficient reaction. The bright yellow GO suspension was washed with HCl (5 vol%) three times and then rinsed with deionized water until the pH value reached 6 after centrifugation. A liquid crystalline aqueous solution containing 150–200 μm wide GO sheets was obtained with a concentration of *ca*. 20 mg ml^{-1}.

Spinning of helical GO and rGO fibers

The as-prepared GO aqueous solution (20 mg mL^{-1}) was coated on a Teflon baseboard and spread into a uniform gel-state film by sliding a Teflon bar over the baseboard surface.[21] The gel thickness was controlled by the number of plies of the adhesive tape wrapped around the Teflon bar ends, which separates the bar and baseboard at a predefined distance. After drying at room temperature, the free-standing GO film was peeled off from the baseboard and cut into long strips with the desired widths by using a roller blade. To spin the fibers, one end of the GO strip was fixed to the shaft of an electrical motor controlled by a DC power supply, while the other end was connected to a metal block which can move freely on a smooth glass. A mist spraying was applied to the GO strip for 30 seconds producing an environmental humidity of 80%. The suspended wet-state GO strip was spun into a straight yarn and then over-twisted into a helical structure like a spring, at 1500 rpm. The helical GO fibers were reduced by HI acid at 90 °C for 12 hours and washed with deionized water to obtain conductive rGO fibers.

Structural characterization

The morphology and structure of helical GO and rGO fibers were characterized by SEM (JEOL JSM-6700F), X-ray diffraction (XRD) with Cu Kα radiation (λ = 1.5406 Å), and Raman spectroscopy (Renishaw-inVia Reflex) using a 514 nm wavelength laser.

Mechanical and electrical measurement

Uniaxial tension and cyclic tests were carried out in a single-column testing instrument (Instron 5843) equipped with 10 N load cells and specially designed grips for fiber-shaped samples. The two ends of a helical GO or rGO fiber were glued onto a paper window by polyvinyl alcohol while keeping the fiber straight, and then installed onto the grips carefully. For tension tests, the elongation rate was set as 1 mm min^{-1}. For cyclic tests, the strain rate was set to be 20% min^{-1} for maximum strains of 10% to 50%. Electrical measurements were performed simultaneously. Silver wires were fixed to the fiber ends by high purity silver paint, and then connected to the digital source meter (Keithley 2635A). Electric current flowing through the fiber during mechanical tests was recorded under a constant bias (1 V), and the two-probe resistance was calculated based on the applied voltage and measured current.

Electrocapillary suction based on helical rGO fibers

The three-electrode system consists of a helical rGO fiber suspended on a copper wire as the working electrode (WE), a commercial Ag/AgCl in 3 M KCl as the reference electrode (RE), and a CNT sponge as the contour electrode (CE).[36] The rGO fibers were cut by using scissors into 1–2 cm long segments to expose internal cavities, and the outer fiber surface was covered by thin PTFE tape to prevent the influence of outside meniscus and a possible evaporation effect. The fiber was suspended under a microbalance (ME36S, Sartorius, Germany) *via* cotton, and placed over a liquid reservoir containing a 1 M KOH aqueous electrolyte. To start the test, the electrolyte reservoir was raised by a motorized laboratory stage to contact the fiber bottom. The mass change of the fiber during imbibition was recorded at the rate of 1 s^{-1}. The formation and development of the outside meniscus contribute to the abrupt mass increase shortly after contact, which has been subtracted from all data. A potential of −1.2 V was purged for 10 seconds, and then the potential was maintained at 0 V for 2 minutes to stabilize the outside meniscus prior to each measurement before the test potential was applied.

Temperature sensors based on helical GO fibers

A helical rGO fiber was placed on a heating station enclosed in the test circuit of a thermal tester (CGS-1TP, Beijing Elite. Tech.). The two fiber ends were connected to a source meter by silver wires and silver paint, under a constant bias of 4 V. First, the test was carried out at room temperature to calculate the initial 2-probe resistance. Then, the resistance change was monitored when the fiber was heated uniformly to target temperatures of 100, 200, and 300 °C, respectively, and the temperature was recorded by the instrument simultaneously. After reaching the target temperature, the resistance was kept stable for certain time and then heating was stopped to let the fiber cool down naturally to room temperature. The relative resistance change during heating and cooling was obtained. This process was repeated to test the cyclic behavior and device stability.

Acknowledgements

The authors greatly acknowledge financial support from the National Natural Science Foundation under grants of NSFC 51325202, 51502267, China Postdoctoral Science Foundation funded project (2015M582200). We thank S. Hu for assistance in electrocapillary tests.

References

1 B. Vigolo, A. Pénicaud, C. Coulon, C. Sauder, R. Pailler, C. Journet, P. Bernier and P. Poulin, *Science*, 2000, **290**, 1331.
2 M. Zhang, K. R. Atkinson and R. H. Baughman, *Science*, 2004, **306**, 1358.
3 K. Koziol, J. Vilatela, A. Moisala, M. Motta, P. Cunniff, M. Sennett and A. Windle, *Science*, 2007, **318**, 1892.
4 D. S. Yu, K. L. Goh, H. Wang, L. Wei, W. C. Jiang, Q. Zhang, L. M. Dai and Y. Chen, *Nat. Nanotechnol.*, 2014, **9**, 555.
5 Z. B. Yang, H. Sun, T. Chen, L. B. Qiu, Y. F. Luo and H. S. Peng, *Angew. Chem., Int. Ed.*, 2013, **125**, 7693.
6 H. H. Cheng, J. Liu, Y. Zhao, C. G. Hu, Z. P. Zhang, N. Chen, L. Jiang and L. T. Qu, *Angew. Chem., Int. Ed.*, 2013, **52**, 10482.
7 H. H. Cheng, Y. Hu, F. Zhao, Z. L. Dong, Y. H. Wang, N. Chen, Z. P. Zhang and L. T. Qu, *Adv. Mater.*, 2014, **26**, 2909.
8 B. Fang, L. Peng, Z. Xu and C. Gao, *ACS Nano*, 2015, **9**, 5214.
9 Z. Xu and C. Gao, *Mater. Today*, 2015, **18**, 480.
10 F. C. Meng, W. B. Lu, Q. W. Li, J. H. Byun, Y. Oh and T. W. Chou, *Adv. Mater.*, 2015, **27**, 5113.
11 H. H. Cheng, C. G. Hu, Y. Zhao and L. T. Qu, *NPG Asia Mater.*, 2014, **6**, e113.
12 F. Zhao, Y. Zhao, H. H. Zhao and L. T. Zhao, *Angew. Chem., Int. Ed.*, 2015, **54**, 14951.
13 Z. Li, Z. Liu, H. Y. Sun and C. Gao, *Chem. Rev.*, 2015, **115**, 7046.
14 Z. Xu and C. Gao, *Nat. Commun.*, 2011, **2**, 571.
15 J. K. Sun, Y. H. Li, Q. Y. Peng, S. C. Hou, D. C. Zou, Y. Y. Shang, Y. B. Li, P. X. Li, Q. J. Du, Z. H. Wang, Y. Z. Xia, L. H. Xia, X. L. Li and A. Y. Cao, *ACS Nano*, 2013, **7**, 10225.
16 R. Jalili, S. H. Aboutalebi, D. Esrafilzadeh, R. L. Shepherd, J. Chen, S. Aminorroaya-Yamini, K. Konstantinov, A. I. Minett, J. M. Razal and G. G. Wallace, *Adv. Funct. Mater.*, 2013, **23**, 5345.
17 Z. Xu and C. Gao, *Acc. Chem. Res.*, 2014, **47**, 1267.
18 G. Q. Xin, T. K. Yao, H. T. Sun, S. M. Scott, D. L. Shao, G. K. Wang and J. Lian, *Science*, 2015, **349**, 1083.
19 Z. L. Dong, C. C. Jiang, H. H. Cheng, Y. Zhao, G. Q. Shi, L. Jiang and L. T. Qu, *Adv. Mater.*, 2012, **24**, 1856.
20 J. H. Li, J. Y. Li, L. F. Li, M. Yu, H. J. Ma and B. W. Zhang, *J. Mater. Chem. A*, 2014, **2**, 6359.
21 R. Cruz-Silva, A. Morelos-Gomez, H. I. Kim, H. K. Jang, F. Tristan, S. Vega-Diaz, L. P. Rajukumar, A. L. Elías, N. Perea-Lopez, J. Suhr, M. Endo and M. Terrones, *ACS Nano*, 2014, **8**, 5959.
22 R. R. Wang, J. Sun, L. Gao, C. H. Xu and J. Zhang, *Chem. Commun.*, 2011, **47**, 8650.
23 M. K. Shin, B. Lee, S. H. Kim, J. A. Lee, G. M. Spinks, S. Gambhir, G. G. Wallace, M. E. Kozlov, R. H. Baughman and S. J. Kim, *Nat. Commun.*, 2012, **3**, 650.
24 H. Sun, X. You, J. Deng, X. L. Chen, Z. B. Yang, J. Ren and H. S. Peng, *Adv. Mater.*, 2014, **26**, 2868.
25 Z. Xu, Z. Liu, H. Y. Sun and C. Gao, *Adv. Mater.*, 2013, **25**, 3249.
26 Z. Xu, Y. Zhang, P. G. Li and C. Gao, *ACS Nano*, 2012, **6**, 7103.
27 Y. Zhao, C. C. Jiang, C. G. Hu, Z. L. Dong, J. L. Xue, Y. N. Meng, N. Zheng, P. W. Chen and L. T. Qu, *ACS Nano*, 2013, **7**, 2406.
28 Y. Cheng, R. R. Wang, J. Sun and L. Gao, *Adv. Mater.*, 2015, **27**, 7365.
29 G. J. Huang, C. Y. Hou, Y. L. Shao, H. Z. Wang, Q. H. Zhang, Y. Q. Li and M. F. Zhu, *Sci. Rep.*, 2014, **4**, 4248.
30 Y. Y. Shang, X. D. He, Y. B. Li, L. H. Zhang, Z. Li, C. Y. Ji, E. Z. Shi, P. X. Li, K. Zhu, Q. Y. Peng, C. Wang, X. J. Zhang, R. G. Wang, J. Q. Wei, K. L. Wang, H. W. Zhu, D. H. Wu and A. Y. Cao, *Adv. Mater.*, 2012, **24**, 2896.
31 Y. Y. Shang, Y. B. Li, X. D. He, S. Y. Du, L. H. Zhang, E. Z. Shi, S. T. Wu, Z. Li, P. X. Li, J. Q. Wei, K. L. Wang, H. W. Zhu, D. H. Wu and A. Y. Cao, *ACS Nano*, 2013, **7**, 1446.
32 Y. B. Li, Y. Y. Shang, X. D. He, Q. Y. Peng, S. Y. Du, E. Z. Shi, S. T. Wu and A. Y. Cao, *ACS Nano*, 2013, **9**, 8128.
33 Z. Xu, H. Y. Sun, X. L. Zhao and C. Gao, *Adv. Mater.*, 2013, **25**, 188.
34 E. Y. Jang, J. Carretero-González, A. Choi, W. J. Kim, M. E. Kozlov, T. Kim, T. J. Kang, S. J. Baek, D. W. Kim, Y. W. Park, R. H. Baughman and Y. H. Kim, *Nanotechnology*, 2012, **23**, 235601.
35 Y. H. Xue, J. Markmann, H. L. Duan, J. Weissmüller and P. Huber, *Nat. Commun.*, 2014, **5**, 4237.
36 Y. H. Xue, Y. B. Yang, H. Sun, X. Y. Li, S. T. Wu, A. Y. Cao and H. L. Duan, *Adv. Mater.*, 2015, **27**, 7241.
37 M. Alava, M. Dubéc and M. Rost, *Adv. Phys.*, 2004, **53**, 83.
38 Z. Liu, Z. Li, Z. Xu, Z. X. Xia, X. Z. Hu, L. Kou, L. Peng, Y. Y. Wei and C. Gao, *Chem. Mater.*, 2014, **26**, 6786.
39 D. C. Marcano, D. V. Kosynkin, J. M. Berlin, A. Sinitskii, Z. Z. Sun, A. Slesarev, L. B. Alemany, W. Lu and J. M. Tour, *ACS Nano*, 2010, **4**, 4806.

